Received: 26 April 2024 | Revised: 6 August 2024 | Accepted: 9 August 2024

DOI: 10.1111/jace.20119

Journal of the American Ceramic Society

RESEARCH ARTICLE

First-principles study of helium incorporation in Pu-$La_2Zr_2O_7$ pyrochlore

Chenguang Liu[1] | **Rongrong Gao**[1] | **Xiaoyi Xia**[1] | **Kunjie Yang**[1] | **Yuelin Liu**[1] | **Pan Yang**[1] | **Qing Peng**[2,3,4] | **Fei Gao**[5,6]

[1]Yantai Key Laboratory of Advanced Nuclear Energy Materials and Irradiation Technology, College of Nuclear Equipment & Nuclear Engineering, Yantai University, Yantai, China

[2]State Key Laboratory of Nonlinear Mechanics, Institute of Mechanics, Chinese Academy of Sciences, Beijing, China

[3]Xinyan Semi Technology Co. Ltd, Wuhan, China

[4]Guangdong Aerospace Research Academy, Guangzhou, China

[5]Department of Nuclear Engineering & Radiological Sciences, University of Michigan, Ann Arbor, Michigan, USA

[6]Department of Materials Science and Engineering, University of Michigan, Ann Arbor, Michigan, USA

Correspondence
Chenguang Liu, College of Nuclear Equipment & Nuclear Engineering, Yantai University, Yantai 264005, China.
Email: liuchg@ytu.edu.cn

Qing Peng, State Key Laboratory of Nonlinear Mechanics, Institute of Mechanics, Chinese Academy of Sciences, Beijing 100190, China.
Email: pengqing@imech.ac.cn

Fei Gao, Department of Nuclear Engineering & Radiological Sciences, University of Michigan, Ann Arbor, MI 48109.
Email: gaofeium@umich.edu

Funding information
Yantai University, Grant/Award Number: HD20B02; Shandong Provincial Natural Science Foundation, Grant/Award Numbers: ZR2021QA028, ZR2023MA045; Shandong Province Young Innovation Team of Higher Education Institutions, Grant/Award Number: 2023KJ242; High-level Innovation Research Institute Program of Guangdong Province, Grant/Award Number: 2020B0909010003; Strategic Priority Research Program of Chinese Academy of Sciences, Grant/Award Number: XDB0620103; National Natural Science Foundation of China, Grant/Award Numbers: 12205248, 12175093, 11875046, 12272378

Abstract

Helium (He) exerts significant influence on the physicochemical, structural, and electronic properties of pyrochlores. This paper reviews recent advancements in computer simulations aimed at stabilizing nuclear waste, focusing on disordered structures of pyrochlores, zirconate pyrochlores, and high-entropy pyrochlores. Using Pu-$La_2Zr_2O_7$ as a case study, we demonstrate how a first-principles approach facilitates the understanding of how He modifies the structural and electronic properties of this system. The incorporation of He interstitials in Pu-$La_2Zr_2O_7$ typically leads to an expansion in lattice constant and volume swelling. Analysis of the formation energies in this system reveals that octahedral interstitial sites or zirconium (Zr) vacancy sites are favored for He occupation, resulting in the formation of substitutional He atoms. The low concentration of He atoms in Pu-$La_2Zr_2O_7$ reduces the formation energy of cation antisite defects. Bader charge analysis indicates that the < Zr-O > bond exerts a greater influence on the irradiation resistance of the He-Pu-$La_2Zr_2O_7$ system compared to the < La-O > bond. Moreover, the capacity for He interstitials increases with higher Pu concentration in the octahedrons.

KEYWORDS
first-principles study, He interstitials, irradiation resistance, pyrochlores

1 | INTRODUCTION

Nuclear energy serves as a stable and clean energy source, playing a pivotal role in achieving the goals of carbon peak and carbon neutralization. Ensuring the safe and efficient disposal of nuclear waste is crucial for the sustainable advancement of nuclear energy.[1–3] Pyrochlore is considered a promising substrate material for immobilizing high-level nuclear waste due to its exceptional chemical durability, high thermal stability, and robust radiation resistance.[4–6] Given the constraints of experimental characterization in terms of temporal and spatial scales, coupled with the hazardous nature of radionuclides, computer simulations have been widely used to probe the physical and chemical properties of pyrochlores. With regard to the application of pyrochlores in the field of nuclear energy, recent advancements in exploring pyrochlores as nuclear waste forms have predominantly focused on the following areas.

1.1 | Current statues of simulations study of pyrochlores for nuclear energy applications

1.1.1 | Local short-range order structure of weberite

Pyrochlores ($A_2B_2O_7$) undergo phase transitions from ordered to disordered (O-D) or amorphous (O-A) phases upon irradiation. A correlation exists between the propensity for phase transitions and energy expenditure associated with cation disordering in pyrochlores. The pyrochlore amorphization tendency intensifies with the escalating energy cost of cation disorder, characterized by the swapping of A and B cations within the pyrochlore structure. Previous studies have elucidated a disordered structure, where cations A and B exchange positions along with anion Frenkel pairs, resulting in a random distribution of oxygen vacancies.[7] However, recent neutron total-scattering experiments have revealed that locally-ordered domains contribute to the formation of large-scale disordered pyrochlore structures. The local-order structure was identified as an orthorhombic weberite model with space group *Ccmm* crystal symmetry. Regarding the underlying mechanism of the formation of the local weberite structure, Zhao et al.[8] studied the order-disorder transition in $A_2Zr_2O_7$(A = La to Er) pyrochlores using first-principles calculations and suggested that the weberite structure can be attributed to the movement of 48*f* oxygen to the nearest vacant 8*a* site. The extent of the phase transition from pyrochlore to weberite depends on the cation properties, is characterized by the oxygen migration ratio. Regarding the stability of weberite, first principles simulations[9] revealed that the weberite-type structure is more energetically stable than the fully ordered pyrochlore structure for most zirconate and hafnate pyrochlores (see Figure 1). For $A_2Ti_2O_7$, the weberite-type structure was stabilized against pyrochlore only in cases with small A ionic radii (A = Lu-Er, as shown in Figure 1).

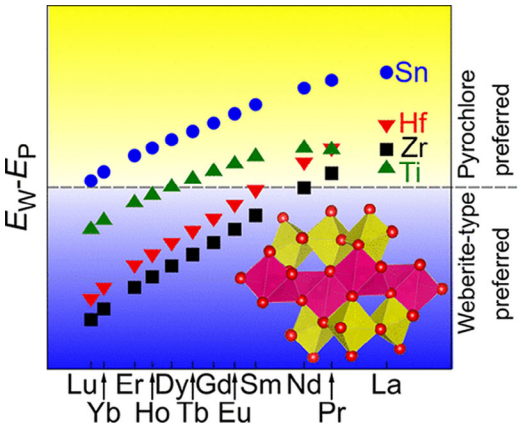

FIGURE 1 Energy difference between weberite-type and pyrochlore for lanthanoid zirconates (black squares), hafnates (red downward triangles), stannates (blue circles), and titanates (green upward triangles). Reproduced from Ref. (9).

Similar conclusions were reached by calculating the formation enthalpies of $Ln_2B_2O_7$ (B = Ti, Sn, Hf, and Zr) compounds in pyrochlore, defect fluorite, and weberite structures using DFT.[10] The defective fluorite phase was unstable in the entire range of the considered compositions, except for the $Ln_2Ti_2O_7$ compound. The weberite phases of $Ln_2Hf_2O_7$ and $Ln_2Zr_2O_7$ were more stable than those of the lanthanides (Ln) after Dy and Gd, respectively.

The connections and distinctions between weberite and pyrochlore with the same chemical formula are presently ambiguous. We performed a comparative analysis of the physical properties of $Gd_2Zr_2O_7$ weberite and pyrochlore using a first-principles method.[11] Our finding revealed that cation antisite defects are more readily formed in the weberite lattice compared to the pyrochlore lattice. The formation of vacancy defects is influenced by the availability of vacant lattice sites for the respective atoms. Furthermore, both weberite and pyrochlore were found to be mechanically stable and exhibited comparably mechanical properties.

1.1.2 | Simulation of high entropy pyrochlore

High-entropy ceramics have attracted increasing interest owing to their enhanced mechanical resilience,

catalytic efficiency, electrical conductivity and thermal stability.[12] High-entropy pyrochlores, a typical high-entropy ceramic, have been studied extensively in terms of their physical properties and radiation tolerance because of their potential applications in thermal barrier coating and nuclear waste disposal.[13–15] A comparative study of the physical properties and radiation tolerance of the B-site high-entropy pyrochlore $Gd_2(Ti_{0.25}Zr_{0.25}Sn_{0.25}Hf_{0.25})_2O_7$ and individual pyrochlores $Gd_2X_2O_7$(X = Ti, Zr, Sn, Hf) was performed using first-principles calculations, and the results showed that high entropy at the B sites lead to lattice distortion and enhanced radiation tolerance.[16] Similar conclusions were confirmed by the experimental measurements and calculated results for $Gd_2(Ti_{0.2}Zr_{0.2}Sn_{0.2}Hf_{0.2}Ta_{0.2})_2O_7$, $Gd_2(Ti_{0.2}Zr_{0.2}Sn_{0.2}Hf_{0.2}Nb_{0.2})_2O_7$[17] and $Gd_2(Ti_{0.25}Zr_{0.25}Hf_{0.25}Ce_{0.25})_2O_7$.[14] As for the high entropy at A sites in pyrochlores, $(Lu_{0.25}Y_{0.25}Eu_{0.25}Gd_{0.25})_2Ti_2O_7$ has been experimentally prepared and irradiated by 800 keV Kr^{2+} ions. The radiation resistance is characterized by irradiation experiments and the calculated antisite defect formation energy, both of which show that the radiation resistance of the high-entropy pyrochlore is between those of $Eu_2Ti_2O_7$ and $Y_2Ti_2O_7$.[18] The radiation resistance and mechanical properties of $(La_{0.2}Nd_{0.2}Sm_{0.2}Eu_{0.2}Gd_{0.2})_2Zr_2O_7$ were also studied using irradiation experiments and molecular dynamics simulations,[19] which revealed that the radiation resistance of this high-entropy pyrochlore was improved. The formation energies of the A-B site cation antisite defects indicate that the high-entropy pyrochlore has a good radiation defect recovery ability compared with the corresponding ternary pyrochlore. The above results indicate that the A and B-site high-entropy effects on the radiation tolerance of pyrochlores are different, and the underlying mechanism was studied by combining experiments and calculations with similar cationic radius ratios. The results demonstrate that bond strength and chemical environment are key factors that lead to different irradiation responses. When the cation radius ratios are similar, the variance in the A-site elements has a similar impact and may slightly improve the radiation tolerance. Conversely, B-site elements significantly influence radiation tolerance.[12]

1.1.3 | Simulation of radionuclides in zirconate pyrochlore

Zirconate pyrochlores are considered leading candidates for the immobilization of Pu and minor actinides.[20,21] Solid solutions involving actinide immobilization have attracted considerable interest.[22–24] Recently, Shen et al.[25] studied defect formation and its effect on the thermodynamic properties of $Pu_2Zr_2O_7$, which was formed by the immobilization of Pu in the $Gd_2Zr_2O_7$ pyrochlore using first-principles calculations. The results revealed that a Pu-Zr antisite is readily forms, resulting in the spontaneous formation of an O_{8a} interstitial defect in $Pu_2Zr_2O_7$. The elastic moduli and Debye temperature decreased because of the formation of vacancies, interstitial or antisite defects in $Pu_2Zr_2O_7$. Their investigation suggested that defects created defects by self-radiation from actinide decay affected the thermophysical properties of $Pu_2Zr_2O_7$. In addition to studying the behavior of uranium and Pu in pyrochlores, a theoretical study of Th accommodation in $Gd_2Zr_2O_7$ has also been carried out by Zhao et al. using density functional theory.[26] The results demonstrate that Th can be incorporated into both Gd and Zr sites in $Gd_2Zr_2O_7$ pyrochlore, and that Th-containing $Gd_2Zr_2O_7$ pyrochlores are more amenable to undergo O-D phase transformation and exhibit stronger radiation tolerance. Xiao et al.[27] studied the effect of Pu incorporation on $La_2Zr_2O_7$ using density functional theory and found that Pu-doped $La_2Zr_2O_7$ pyrochlore improved the irradiation resistance. Moreover, both La and Zr atoms can be replaced by Pu and form $La_{2-y}Pu_yZr_2O_7$ and $La_2Zr_{2-y}Pu_yO_7$ ($0 \le y \le 2$) solid solutions. The same process also occurs in $Gd_2Zr_2O_7$, where both Gd and Zr atoms can be replaced by Li et al.[28] studied the mechanical and electronic properties of $Gd_2Zr_2O_7$ containing Pu atoms using density functional theory and the Hubbard U correction (DFT+U) method, and found that Pu is mechanically stable at Gd and Zr sites. Zhang et al.[29] simulated the microstructural evolution of $Pu_2Zr_2O_7$ and $La_2Zr_2O_7$ under electron radiation using ab initio molecular dynamics. The results showed that the irradiation tolerance of $Pu_2Zr_2O_7$ is lower than that of $La_2Zr_2O_7$.

1.1.4 | Behavior of helium in pyrochlore

Helium (He) is typically generated during the long-term geological disposal of spent nuclear fuel, causing swelling and impacting multiple physical properties of the solid.[30] The critical concentration of 4.6 at.% required for the formation of He bubbles in $Gd_2Zr_2O_7$ pyrochlore is determined by irradiation with Au and He ions. The individual bubbles slightly increase the lattice swelling, while the bubble chains reduce the lattice strain.[31] Thus, the behavior of He in pyrochlore should not be ignored, henceforth attracting significant attention in theoretical simulations. First-principles calculations have demonstrated that He preferably occupies the octahedral interstitial sites in the $Y_2Ti_2O_7$ pyrochlore lattice, wherein the presence of He atoms can alter the crystal structure and chemical bond

characteristics.[32] The same authors recently reported a systematic study on the behavior of He in $A_2B_2O_7$ (A = La or Gd, B = Zr or Sn) pyrochlores using a first-principles approach.[33–35] The formation energies indicated that the octahedral interstitial site was the most stable site occupied by He. The low accumulation of He atoms causes small lattice swelling and has little effect on the mechanical properties of pyrochlores. However, the presence of He results in a decrease in the formation energy of cation antisite defects, which usually portends the order-to-disorder phase transition and is easier than in pure pyrochlore. In the actual geological disposal environment of spent nuclear fuel, the coexistence of He and radionuclides such as Pu is common. However, an atomistic study of this mixture remains elusive.

As an example, we employed the first-principles method in subsequent sections to study a He-Pu-$La_2Zr_2O_7$ system, and systematically analyze the effect of He atoms on its structural and electronic properties. Based on these results, the effect of He on the radiation resistance of the Pu-$La_2Zr_2O_7$ pyrochlore is discussed from the perspective of the cation antisite defect formation energy.

2 | METHODOLOGY

The Vienna ab initio Simulation Package (VASP) was used to perform all the calculations in this study.[36–39] The interaction between ions and electrons is described by the projector-augmented-wave (PAW),[40,41] and the generalized gradient approximation (GGA) from Perdew-Burke-Ernzerhof (PBE)[42] is used to describe the exchange-correlation functional of the valence electrons. In this study, the electronic configurations of He, La, Zr, O, and Pu were $1s^2$, $5s^25p^65d^16s^2$, $4s^24p^64d^25s^2$, $2s^22p^4$, and $6s^27s^26p^66d^25f^4$, respectively. The strongly correlated f electrons of Pu were modified by the parameter $U_{eff} = 4$ eV based on the Hubbard U correction.[27] A $2 \times 2 \times 2$ k-point sampling pattern in reciprocal space was employed with a cutoff energy of 600 eV for the plane-wave basis sets. The convergence criterion of total energy and total force was 10^{-4} eV and 10^{-3} eV/Å, respectively.

3 | RESULTS AND DISCUSSION

3.1 | Structural characteristics

The convoluted crystal structure of pyrochlore is usually described as a fluorite superstructure of, with an ideal structural formula of $A_2B_2O_7$ and a space group of Fd-3m.[43] All the atoms were in special positions, except for oxygen, which occupied the 48f sites. Therefore, the pyrochlore structure can be completely described by two independent parameters: the lattice parameter a_0 and the O_{48f} fractional coordinates x_{O48f}.[43] In pyrochlores, x_{O48f} is closely correlated with the degree of structural disorder, ranging from 0.3125 to 0.375.[43] When $x = 0.3125$, the structure is an ideal pyrochlore, the cations at site B form an ideal octahedron, and the cations at site A are in the center of the twisted cubic coordination. When $x = 0.375$, the crystal have a defective fluorite structure, the A-position cations were in the center of the regular cube with a coordination number of 8, and the B-position cations were in the center of the highly distorted octahedron. As x_{O48f} approaches 0.375, the pyrochlore becomes closer to a disordered fluorite structure and exhibits stronger radiation resistance.[44–47] Figure 2 shows a schematic of the $La_2Zr_2O_7$ pyrochlore. The relaxed lattice constants a_0 and x_{O48f} and bond distances are summarized in Table 1 and are in reasonable agreement with other theoretical and experimental values.[27,35]

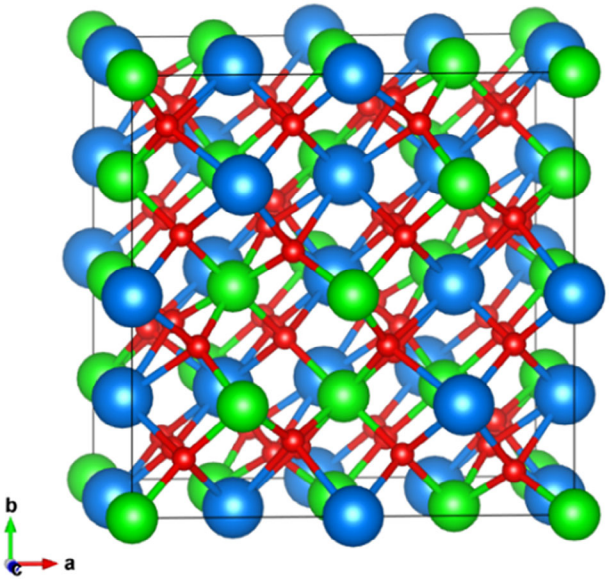

FIGURE 2 Schematic diagram of $La_2Zr_2O_7$ pyrochlore, where blue, green and red spheres represent lanthanum (La), zirconium (Zr), and oxygen (O), respectively.

A La atom was replaced by a Pu atom in a $La_2Zr_2O_7$ lattice cell with 88 atoms, resulting in a Pu-$La_2Zr_2O_7$ system in Figure 3A. To analyze the influence of single He interstitials on the Pu-$La_2Zr_2O_7$ system, eight He interstitial sites were considered. Their configurations are shown in Figure 3B–I. Complete structural relaxation was performed on the Pu-$La_2Zr_2O_7$ and He-Pu-$La_2Zr_2O_7$ pyrochlore systems. Table 1 lists the volumes, lattice constants, x_{O48f} and bond lengths of the two systems. The He interstitials in the middle of the two Zr atoms were transferred to the tetrahedral position after relaxation. Therefore, He was treated as a tetrahedral interstitial in

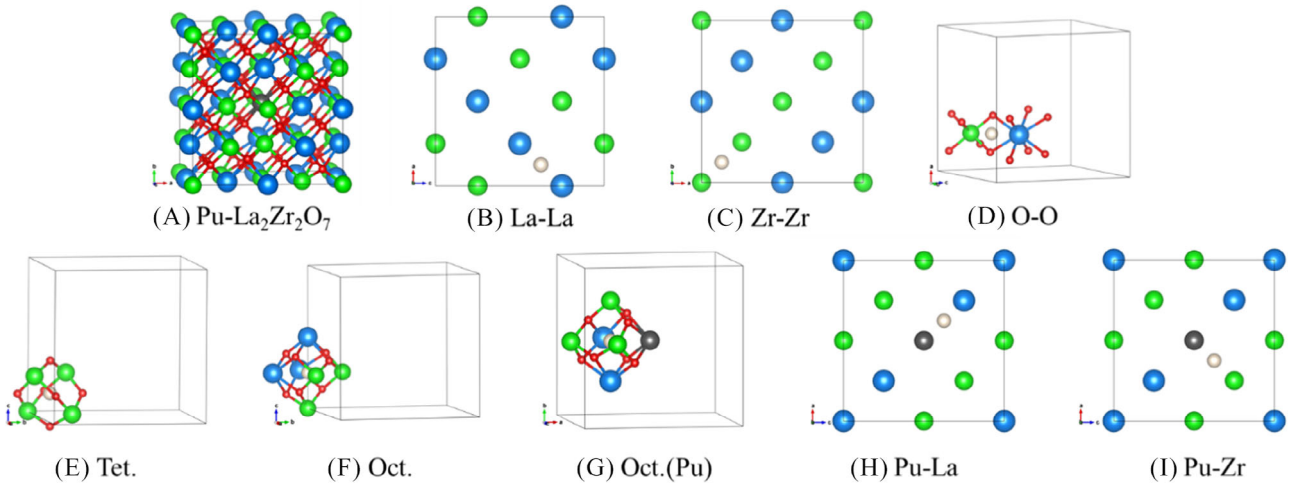

FIGURE 3 Configurations of different interstitial positions of He in Pu-$La_2Zr_2O_7$. (A) Pu-$La_2Zr_2O_7$ system; (B) He interstitial located at the middle between two lanthanum atoms; (C) He interstitial located at the middle of two zirconium atoms; (D) He interstitial located at the middle of two oxygen; atoms (E) He at tetrahedral position; (F) He at octahedral position; (G) He at the octahedral position consisting of Pu; (H) He interstitial located at the middle of plutonium and lanthanum atom; (I) He interstitial located at the middle of plutonium and zirconium atom. The black, white, blue, green, and red spheres represent Pu, He, La, Zr, and O, respectively.

all subsequent analyses. After He interstitial introduction, lattice swelling was observed, and the volume of the He-Pu-$La_2Zr_2O_7$ system increases by 2.33% (He in the La-La interstitial position), 2.57% (He in the Tet. interstitial position), 3.05% (He in the O-O interstitial position), 2.41% (He in the Pu-La interstitial position), 3.13% (He in the Pu-Zr interstitial position), 2.49% (He in the Oct. interstitial position), and 2.57% (He in the Oct.(Pu) interstitial position). The incorporation of He results in the increase of the bond length of $< \text{La-O}_{8b} >$ and $< \text{Pu-O}_{8b} >$. Other chemical bonds were also affected by the incorporation of He, as shown in Table 1. The increased x_{O48f} reveals that the He-Pu-$La_2Zr_2O_7$ systems are closer to a disordered fluorite structure, which means that the incorporation of He may lead to structural distortion and enhance the radiation resistance of the system.[44,45]

3.2 | The preferable location of He in Pu-$La_2Zr_2O_7$

The formation energy is commonly used to evaluate the relative stability of interstitial atoms in compounds.[32,35,48,49] The configuration with a lower formation energy exhibited better structural stability. The formation energy of each configuration of He-Pu-$La_2Zr_2O_7$ is calculated using the following formula[49]:

$$E_f^{He(Int)} = E_{He-Pu-La_2Zr_2O_7} - E_{Pu-La_2Zr_2O_7} - E_{He}.$$

Here, $E_{He-Pu-La_2Zr_2O_7}$ is the total energy of the relaxed Pu-$La_2Zr_2O_7$ system with a He interstitial; $E_{Pu-La_2Zr_2O_7}$ is the total energy of the relaxed pure Pu-$La_2Zr_2O_7$ system, and E_{He} is the ground-state energy of the isolated He atom. Vacancy defects are produced in the lattice structures of pyrochlores under extreme conditions.[50] Therefore, the formation energy of Pu-$La_2Zr_2O_7$ with a He atom at a pre-existing vacancy can be calculated using the following formula[49]:

$$E_f^{He(Vac)} = E_{He+Vac} - E_{Vac} - E_{He}.$$

Here, E_{He+Vac} is the total energy of the Pu-$La_2Zr_2O_7$ system with a He atom occupying a pre-existing vacancy. E_{Vac} denotes the total energy of the Pu-$La_2Zr_2O_7$ system containing vacancy defects.

The formation energies of He at the Pu-$La_2Zr_2O_7$ interstitial and vacancy sites are listed in Table 2. The O-O and Pu-Zr interstitial sites are the most unstable interstitial sites for He atom to occupy due to the highest formation energy of $E_f^{He(Int)} = 3.08$ eV and 2.97 eV, respectively, which is consistent with the maximum volume change of these two cases, as described in Section 3.1. He atom prefers to occupy the octahedral interstitial sites in Pu-$La_2Zr_2O_7$ system because the smallest formation energy for Oct. and Oct.(Pu) is 1.96 eV and 1.97 eV, respectively. In terms of the He formation energy at a vacancy site, the Zr ($E_f^{He(Vac)} = 1.31\ eV$) and La vacancy sites ($E_f^{He(Vac)} = 1.44\ eV$) are the most preferred sites for a He atom to occupy. The most unstable vacancy site for a He atom is the O_{8b} vacancy site, with a formation energy of $E_f^{He(Vac)} = 3.97$ eV. The formation energy for He in the Pu-$La_2Zr_2O_7$ system and pure $La_2Zr_2O_7$ pyrochlore[35] in Table 2 shows that the existence of a Pu atom in the $La_2Zr_2O_7$ pyrochlore has very

TABLE 1 Results of the volume (nm^3), x_{O48f}, lattice constant a_0 (Å) and bond length (Å), compared with available theoretical and experimental results.

	V(nm^3)	x_{O48f}	a_0 (Å)	d < La-O_{48f} > (Å)	d < La-O_{8b} > (Å)	d < Zr-O_{48f} > (Å)	d < Pu-O_{8b} > (Å)	d < Pu-O_{48f} > (Å)
$La_2Zr_2O_7$	1.248	0.333	10.765	2.620	2.331	2.101		
Theory[27,35]	1.259	0.3338	10.797	2.620	2.34	2.11		
		0.3346	10.696	2.589	2.316	2.096		
Exp.[43]		0.332	10.805	2.635	2.339	2.105		
Pu-$La_2Zr_2O_7$	1.246	0.333	10.761	2.619	2.330	2.100	2.315	2.603
La-La	1.275	0.334	10.846	2.690	2.369	2.192	2.349	2.515
Tet.	1.278	0.336	10.851	2.606	2.351	2.15	2.335	2.628
O-O	1.284	0.330	10.868	2.580	2.367	2.096	2.365	2.531
Pu-La	1.274	0.335	10.837	2.647	2.376	2.096	2.365	2.670
Pu-Zr	1.285	0.335	10.875	2.640	2.393	2.098	2.385	2.636
Oct.	1.277	0.334	10.850	2.577	2.349	2.112	2.334	2.627
Oct.(Pu)	1.278	0.333	10.852	2.674	2.373	2.118	2.357	2.654

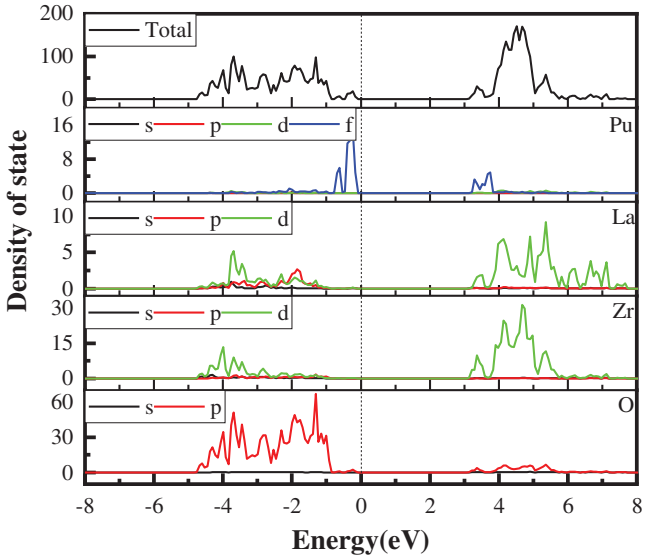

FIGURE 4 Total density of states and partial density of states for pure Pu-$La_2Zr_2O_7$ system.

little effect on the preferred site for He occupation compared with the case of pure $La_2Zr_2O_7$. However, the higher formation energy of He in Pu-$La_2Zr_2O_7$ system means that it is more difficult for He to occupy pre-existing vacancies or interstitial sites.

3.3 | Electronic properties

The electronic structure of pyrochlore always affects the physical and structural properties.[51,52] In this work, the partial density of states (PDOS) and Bader charge were calculated to analyze the electronic structure of He in the Pu-$La_2Zr_2O_7$ system.[53–56] The total density of states (TDOS) and PDOS of the Pu-$La_2Zr_2O_7$ system near the Fermi level are shown in Figure 4. The results showed that the valence band was mainly contributed by the O-2p states. The valence band maximum (VBM) was predominantly determined by the Pu-5f and O-2p states. The conduction band minimum (CBM) is attributed to the Pu-5f, Zr-4d, and O-2p orbitals. In addition, the hybridization of Zr-4d and O-2p was significantly stronger than that of La-5d, Pu-5f, and O-2p. In addition, the difference in the partial density of states (PDOS) between the He-Pu-$La_2Zr_2O_7$ and Pu-$La_2Zr_2O_7$ systems was calculated using the following formula:

$$\Delta\mathrm{PDOS} = \mathrm{PDOS}_{He-Pu-La_2Zr_2O_7} - \mathrm{PDOS}_{Pu-La_2Zr_2O_7}.$$

The calculation results are shown in Figure 5, where only the electron orbitals with substantial changes are listed. The zero, positive, and negative values indicate the

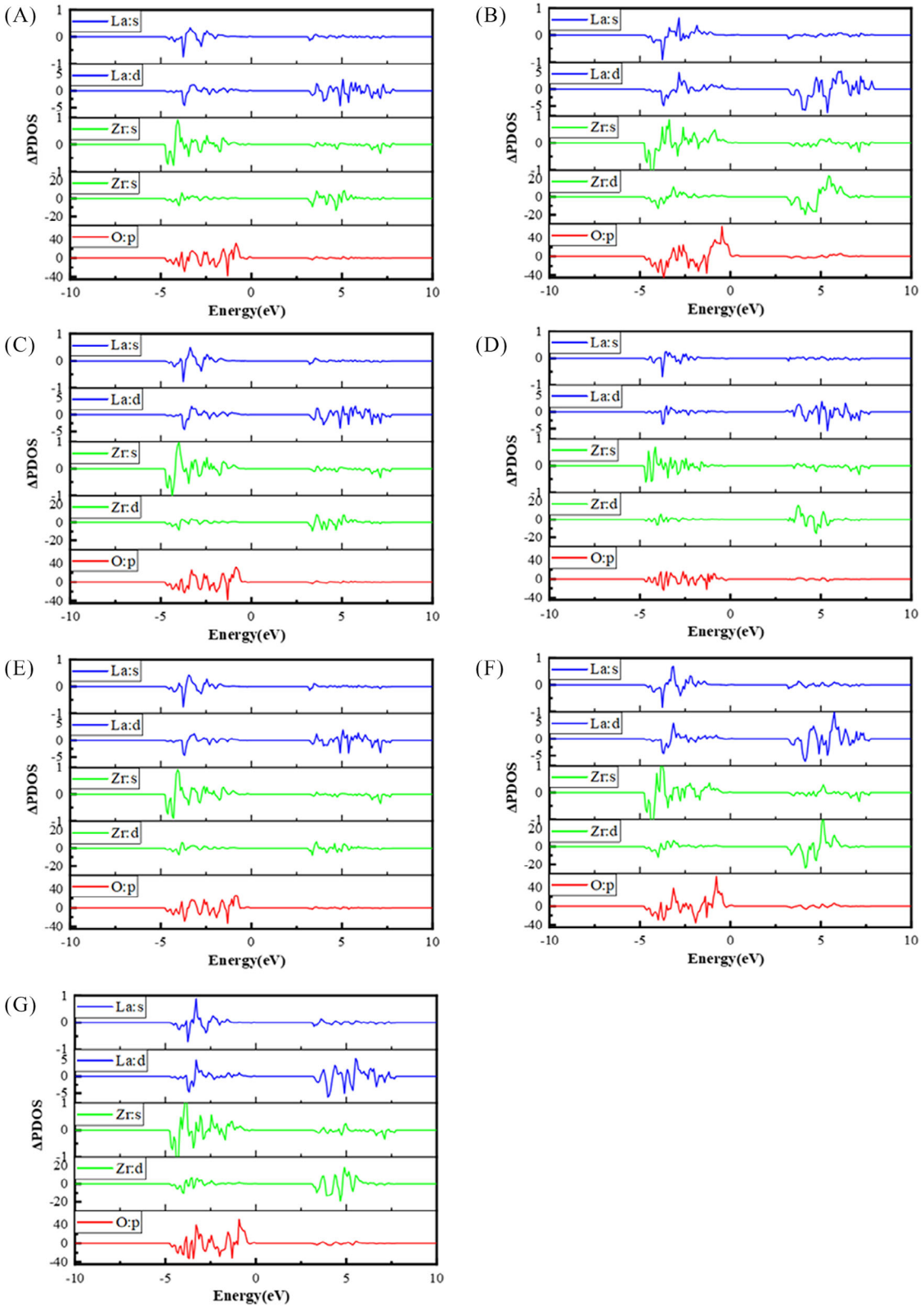

FIGURE 5 The difference of partial density of states (ΔPDOS) of He at different interstitial positions: (A) La-La interstitial; (B) Tet. Interstitial; (C) O-O interstitial; (D) Pu-La interstitial; (E) Pu-Zr interstitial; (F) Oct. interstitial; (G) Oct. (Pu) interstitial.

TABLE 2 Formation energy of He atoms at different interstitial positions($E_f^{He(Int)}$) and preexisting vacancy positions($E_f^{He(Vac)}$).

Formation energy	$E_f^{He(Vac)}$				$E_f^{He(Int)}$						
Site	vLa	vZr	vO_{48f}	vO_{8b}	La-La	O-O	Tet.	Pu-La	Pu-Zr	Oct.	Oct.(pu)
Pu-$La_2Zr_2O_7$	1.44	1.31	2.23	3.97	2.33	3.08	2.37	2.30	2.97	1.96	1.97
$La_2Zr_2O_7$[35]	0.33	0.37	1.57	3.11	1.80	2.69	2.01			1.60	

TABLE 3 Average Bader charges of Pu, La, and Zr in Pu-$La_2Zr_2O_7$ and He-Pu-$La_2Zr_2O_7$ systems.

Average Bader charge (|e|)	Pu-$La_2Zr_2O_7$	He-Pu-$La_2Zr_2O_7$						
		La-La	Tet.	O-O	Pu-La	Pu-Zr	Oct.	Oct.(Pu)
Pu	2.082	2.082	2.090	2.084	2.069	2.031	2.090	2.089
La	2.122	2.094	2.124	2.103	2.097	2.107	2.117	2.113
Zr	2.552	2.568	2.564	2.573	2.570	2.573	2.564	2.569

same, increased, and decreased PDOS, respectively, compared to He-Pu-$La_2Zr_2O_7$ with Pu-$La_2Zr_2O_7$. The obvious distinctions are observed in the s and d orbitals of La, the d orbitals of Zr, and the *p* orbitals of O, which indicate that there are obvious changes in the bonding properties of < La-O > and < Zr-O > bonds.

Using the optimized structure, we calculated the Bader charge of each ion in the He-Pu-$La_2Zr_2O_7$ system and the results are summarized in Table 3. Because of the similar ionic radii of La^{3+} and Pu^{3+}, the incorporation of Pu had little effect on the charge distribution in the entire system. The average Bader charges of Zr and La increased and decreased slightly, respectively. The < Zr-O > bond covalency is reduced, but the < La-O > covalency of the bond is enhanced. The strength of the covalent bond is closely correlated with the radiation resistance of pyrochlore.[35] Irradiation-induced defects are almost immobile in pyrochlores and accumulate because of their robust network of covalent bonds, which ultimately increases the probability of lattice amorphization.[57] Thus the < Zr-O > bond has a greater effect on the irradiation resistance of the He-Pu-$La_2Zr_2O_7$ pyrochlore system than the < La-O > bond.

3.4 | Cation antisite defect formation energy and binding energy

Pyrochlores have better irradiation resistance when they approach a disordered fluorite structure.[51,52] Pyrochlores with lower cation antisite defect formation energies are more prone to undergo order-to-disorder phase transitions and maintain better radiation tolerance.[52,58–61] To assess the influence of the incorporation of He atoms on the radiation tolerance of the Pu-$La_2Zr_2O_7$ system, the formation energies of the cation antisite defects were calculated, and the results are listed in Table 4. A cation antisite defect was formed by exchanging two adjacent cations in the pyrochlore.[62] The cation antisite defect formation energy can be calculated as follows[35]:

$$E_f^{CA} = E_{tot}^{CA} - E_{tot},$$

where E_{tot}^{CA} is the total energy of the He-Pu-$La_2Zr_2O_7$ system with a cation antisite defect, and E_{tot} is the total energy of the He-Pu-$La_2Zr_2O_7$ system. The cation antisite defect formation energy of the He-doped Pu-$La_2Zr_2O_7$ system is lower than that of the Pu-$La_2Zr_2O_7$ system, suggesting that the incorporation of He enhances the radiation tolerance of the system. Pu-$La_2Zr_2O_7$ system with He interstitials had a lower cation antisite defect formation energy than the pure $La_2Zr_2O_7$ system.[35] These findings demonstrate that the Pu-$La_2Zr_2O_7$ system performs better than $La_2Zr_2O_7$ in radiative environments.

In the process of geological disposal of high-level nuclear waste, the accumulation of He atoms results in an increased concentration of He and affects the physical properties of the waste form.[30] Based on the fact that He atoms prefer to occupy the octahedral interstitial sites, we considered He accumulation by adding He into the octahedral interstitial sites of the Pu-$La_2Zr_2O_7$ system up to a concentration of 3.3 at. % (containing three He atoms in the system) is reached. The cation antisite defect formation energies of the different configurations of the He-Pu-$La_2Zr_2O_7$ systems (shown in Figure 6) were studied, and the results are listed in Table 5. The Pu-$La_2Zr_2O_7$ system with a low concentration of He interstitials has a lower cation antisite defect formation energy than the Pu-$La_2Zr_2O_7$ system, which indicates that a low concentration of He may improve the irradiation resistance of the Pu-$La_2Zr_2O_7$ system; however, this conclusion is only based on the antisite defect formation energy.

TABLE 4 Cation antisite defect formation energy of He at different interstitial sites.

System	Site	Antisite defect formation energy (eV)	System	Site	Antisite defect formation energy (eV)
Pure Pu-$La_2Zr_2O_7$		4.172	Pure $La_2Zr_2O_7$		2.410
He-Pu-$La_2Zr_2O_7$	La-La	1.788	He-$La_2Zr_2O_7$[35]	La-La	1.887
	Zr-Zr	2.204		Zr-Zr	2.317
	O-O	2.613		O-O	0.780
	Oct.	1.883		Oct.	1.931
	Pu-La	2.084			
	Pu-Zr	1.208			
	Oct.(Pu)	2.402			

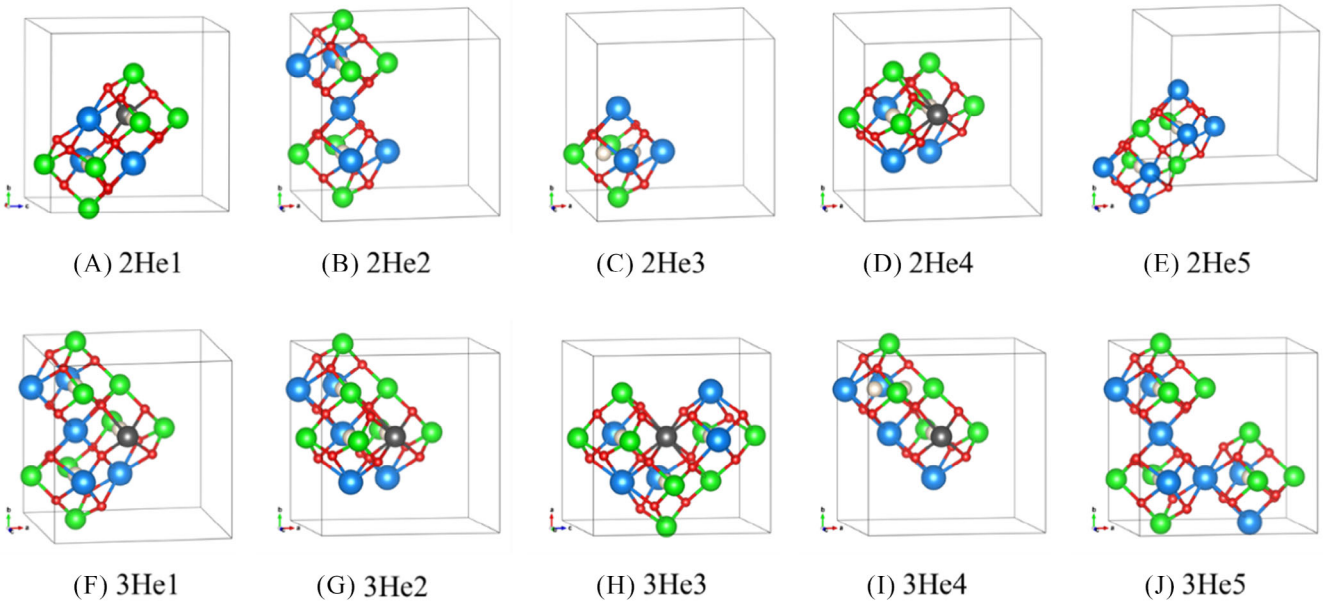

FIGURE 6 Atomic octahedral configurations with different He concentrations in Pu-$La_2Zr_2O_7$ with two He atoms: (A) 2He1, (B) 2He2, (C) 2He3, (D) 2He4, (E) 2He5; three He atoms: (F) 3He1, (G) 3He2, (H) 3He3, (I) 3He4, (J) 3He5.

TABLE 5 Cation antisite defect formation energy of various configurations at octahedral interstitial sites with different He concentrations. The corresponding structures are shown in Figure 6.

Configuration	Cation antisite defect formation energy (eV)	Configuration	Cation antisite defect formation energy (eV)
2he1	1.765	3he1	2.004
2he2	1.933	3he2	2.326
2he3	2.015	3he3	1.740
2he4	1.874	3he4	0.970
2he5	2.091	3he5	1.894

To assess the effect of the Pu concentration on the stability of He clusters, one or two La atoms in the octahedron were replaced by Pu atoms to increase the concentration of Pu in the He-Pu-$La_2Zr_2O_7$ systems and the configurations as shown in Figure 7. The binding energy was calculated using the following formula[63]:

$$E^b_{nHeI} = [E_{I+nHe} - E_{I+(n-1)He}] - [E_{bulk+1He} - E_{bulk}],$$

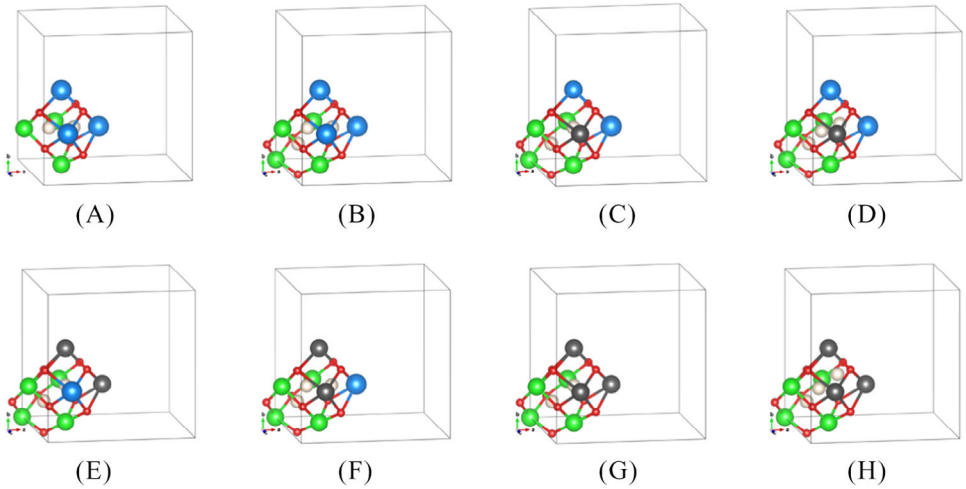

FIGURE 7 Configurations of He-$La_2Zr_2O_7$ and He-Pu-$La_2Zr_2O_7$ systems. He-$La_2Zr_2O_7$ system: (A) 2He, (B) 3He; He-Pu-$La_2Zr_2O_7$ system: (C) 1Pu2He, (D) 1Pu3He, (E) 2Pu2He, (F) 2Pu3He, (G) 3Pu2He, (H) 3Pu3He.

TABLE 6 The binding energies of the He-$La_2Zr_2O_7$ and He-Pu-$La_2Zr_2O_7$ systems.

Configuration		Binding energy (eV)
He-$La_2Zr_2O_7$	2He	0.124
	3He	4.631
He-Pu-$La_2Zr_2O_7$	1Pu2He	−0.627
	1Pu3He	−0.052
	2Pu2He	−0.647
	2Pu3He	−0.056
	3Pu2He	−0.586
	3Pu3He	12.994

here, E_{I+nHe} and $E_{I+(n-1)He}$ denote the total energy of the Pu-$La_2Zr_2O_7$ system with n He atoms and n-1 He atoms at the octahedral interstitial sites, respectively. $E_{bulk+1He}$ represents the total energy of the Pu-$La_2Zr_2O_7$ system with one He atom at the octahedral interstitial site. E_{bulk} is the total energy of the pure Pu-$La_2Zr_2O_7$ system in the absence of He. The calculation results are listed in Table 6. A negative binding energy indicates that the He cluster is energetically stable, whereas a positive binding energy indicates that the cluster is less stable at interstitial sites.[63] For the pure $La_2Zr_2O_7$ system, the binding energies of the He clusters containing two and three He atoms in the octahedral interstitial sites were 0.124 eV and 3.908 eV, respectively, suggesting that these He clusters were unstable. For the He-Pu-$La_2Zr_2O_7$ system, except for 3Pu3He, as shown in Figure 7H, all values of the binding energy are negative, which indicates that He clusters are more stable in the octahedron consisting of Pu and Zr atoms than in the octahedron consisting of La and Zr atoms. The He interstitial capacity increased with increasing Pu concentration in the octahedrons. However, a capacity limit is also apparent. For example, the third trapped He atom in an octahedron containing three Pu atoms (3Pu3He, as shown in Figure 7H) is energetically unfavorable, with a sharply increased binding energy E^b_{3HeI} = 12.994 eV.

4 | CONCLUSIONS

This work has summarized the current advancements in the study of pyrochlores as nuclear waste forms, encompassing $A_2Zr_2O_7$ (A = La to Er) weberite structure, zirconate pyrochlore, and high-entropy pyrochlores, along with the application of the first-principles method to calculate their defect properties. Specifically, the Pu-$La_2Zr_2O_7$ pyrochlore was employed to demonstrate how the first-principles approach aids in to understanding the impact of He on its structural and electronic properties. The structural properties, defect formation energy, electronic properties, and cation antisite defect formation energy of He in the Pu-$La_2Zr_2O_7$ system were studied using first-principles density functional theory calculations. The incorporation of He into the Pu-$La_2Zr_2O_7$ system led to an expansion in lattice constant and volume. Analysis of the formation energy indicated that the preferred sites for He occupancy in the Pu-$La_2Zr_2O_7$ system were octahedral interstitial sites or preexisting Zr vacancy sites. Furthermore, the increased x_{O48f} and decreased cation antisite defect formation energy after He incorporation suggested a propensity for order-to-disorder phase transition in He-Pu-$La_2Zr_2O_7$ systems under irradiation. Further, Bader charge analysis indicated that the irradiation resistance of the He-Pu-$La_2Zr_2O_7$ pyrochlore system was significantly affected

by the < Zr-O > bond compared to the < La-O > bond. Finally, with an increase in Pu concentration, the capacity of octahedral interstitials to accommodate He also rose.

ACKNOWLEDGMENTS

This work is supported by the National Natural Science Foundation of China (grant number 12205248, 12175093, 11875046), the start-up fund from Yantai University to C.L. (grant number HD20B02.), Shandong Provincial Natural Science Foundation (grant number ZR2021QA028, ZR2023MA045) and Development Plan of Shandong Province Young Innovation Team of Higher Education Institutions (grant number2023KJ242). Q. P. would like to acknowledge the support provided by National Natural Science Foundation of China (grant number 12272378), High-level Innovation Research Institute Program of Guangdong Province (grant number 2020B0909010003), and Strategic Priority Research Program of Chinese Academy of Sciences (grant number XDB0620103).

ORCID

Chenguang Liu https://orcid.org/0000-0002-2943-1774

REFERENCES

1. Ringwood AE, Oversby VM, Kesson SE, Sinclair W, Ware N, Hibberson W, et al. Immobilization of high-level nuclear reactor wastes in SYNROC: A current appraisal. Nucl Chem Waste Manag. 1981;2(4):287–305.
2. Hench LL, Clark DE, Campbell J. High level waste immobilization forms. Nucl Chem Waste Manag. 1984;5(2):149–73.
3. Hecker SS. Preventing nuclear weapon proliferation as nuclear power expands. MRS Bull. 2011;33(4):340–42.
4. Kamizono H, Hayakawa I, Muraoka S. Durability of zirconium-containing ceramic waste forms in water. J Am Ceram Soc. 2005;74(4):863–64.
5. Hayakawa I, Kamizono H. Durability of an $La_2Zr_2O_7$ waste form containing various amounts of simulated HLW elements. J Nucl Mater. 1993;202(1-2):163–68.
6. Banerjee D, Parayil RT, Gupta SK, Modak B, Banerjee K, Mohapatra M. A comparative study on pyrochlore phase formation in $La_2Zr_2O_7$ in microscopic and macroscopic scale. J Radioanal Nucl Chem. 2023.
7. Sickafus KE, Grimes RW, Valdez JA, Cleave A, Tang M, Ishimaru M, et al. Radiation-induced amorphization resistance and radiation tolerance in structurally related oxides. Nat Mater. 2007;6(3):217–23.
8. Zhao F, Hu S, Xu C, Xiao H, Zhou X, Zu X, et al. Probing local site disorder in zirconate pyrochlores. Ceram Int. 2023;49(11, Part B):18432–41.
9. Matsumoto U, Ogawa T, Kitaoka S, Moriwake H, Tanaka I. First-principles study on the stability of weberite-type, pyrochlore, and defect-fluorite structures of $A_2^{3+}B_2^{4+}O_7$ (A = Lu^{3+}–La^{3+}, B = Zr^{4+}, Hf^{4+}, Sn^{4+}, and Ti^{4+}). J Phys Chem C. 2020;124(37):20555–62.
10. Kowalski PM. Formation enthalpy of $Ln_2B_2O_7$-type (B = Ti,Sn,Hf,Zr) compounds. Scr Mater. 2020;189:7–10.
11. Liu C, Gao R, Xia Y, Xia X, Shi T, Peng Q, et al. A comparative first-principle study on the physical properties of $Gd_2Zr_2O_7$ weberite and pyrochlore. Comput Mater Sci. 2024;245:113285.
12. Li Y, Lei Y, Xiao H, Zhao S, Wang Y, Cao Z, et al. Different mechanisms of A-site and B-site high entropy effect on radiation tolerance of pyrochlores. J Mater Sci Technol. 2024.
13. Li F, Zhou L, Liu Ji-X, Liang Y, Zhang G-J. High-entropy pyrochlores with low thermal conductivity for thermal barrier coating materials. J Adv Ceram. 2019;8(4):576–82.
14. Wang Z, Zhu C, Wang H, Wang M, Liu C, Yang D, et al. Preparation and irradiation stability of $A_2B_2O_7$ pyrochlore high-entropy ceramic for immobilization of high-level nuclear waste. J Nucl Mater. 2023;574:154212.
15. Zhou L, Li F, Liu J-X, Sun S-K, Liang Y, Zhang G-J. High-entropy $A_2B_2O_7$-type oxide ceramics: a potential immobilising matrix for high-level radioactive waste. J Hazard Mater. 2021;415:125596.
16. Liu C, Peng Q, Shi T, Gao F, Li Y. Physical properties and radiation tolerance of high-entropy pyrochlores $Gd_2(Ti_{0.25}Zr_{0.25}Sn_{0.25}Hf_{0.25})_2O_7$ and individual pyrochlores $Gd_2X_2O_7$ (X = Ti, Zr, Sn, Hf) from first principles calculations. Scr Mater. 2022;220:114898.
17. Matović B, Maletaskic J, Maksimović VM, Zagorac J, Lukovic A, Zeng Y-P, et al. Heavily doped high-entropy $A_2B_2O_7$ pyrochlore. Process Appl Ceram. 2023;17(2):113–17.
18. Wang H, Zhu C, He C, Yang D, Li Y. DFT+U study and in-situ TEM investigation of high-entropy titanate pyrochlore $(Lu_{0.25}Y_{0.25}Eu_{0.25}Gd_{0.25})_2Ti_2O_7$. J Eur Ceram Soc. 2022;42(16):7546–52.
19. Wang Z, Zhou L, Liu C, Li Y. The irradiation resistance and mechanical properties of the high-entropy zirconate pyrochlore $(La_{0.2}Nd_{0.2}Sm_{0.2}Eu_{0.2}Gd_{0.2})_2Zr_2O_7$. Nucl Instrum Methods Phys Res, Sect B. 2024;549:165285.
20. Mandal B, Pandey M, Tyagi A. $Gd_2Zr_2O_7$ pyrochlore: potential host matrix for some constituents of thoria based reactor's waste. J Nucl Mater. 2010;406(2):238–43.
21. Wang SX, Begg BD, Wang LM, Ewing RC, Weber WJ, Kutty KVG. Radiation stability of gadolinium zirconate: a waste form for plutonium disposition. J Mater Res. 1999;14(12):4470–73.
22. Patwe S, Tyagi A. Solubility of Ce^{4+} and Sr^{2+} in the pyrochlore lattice of $Gd_2Zr_2O_7$ for simulation of Pu and alkaline earth metal. Ceram Int. 2006;32(5):545–48.
23. Williford R, Weber W. Computer simulation of Pu^{3+} and Pu^{4+} substitutions in gadolinium zirconate. J Nucl Mater. 2001;299(2):140–47.
24. Williford RE, Begg BD, Weber WJ, Hess NJ. Computer simulation of Pu^{3+} and Pu^{4+} substitutions in zircon. J Nucl Mater. 2000;278(2-3):207–11.
25. Shen H, Li M, Li P, Xiao H, Zhang H, Zu X. Defect formation and its effect on the thermodynamic properties of $Pu_2Zr_2O_7$ pyrochlore: a first-principles study. J Am Ceram Soc. 2021;104(5):2301–12.
26. Zhao F, Xiao H, Zhang H, Li P, Shen H, Zu X. An abnormal incorporation behavior of Th in $Gd_2Zr_2O_7$: a first-principles study. J Am Ceram Soc. 2020;103(3):1846–53.
27. Xiao HY, Jiang M, Zhao FA, Liu ZJ, Zu XT. Thermal and mechanical stability, electronic structure and energetic

properties of Pu-containing pyrochlores: $La_{2-y}Pu_yZr_2O_7$ and $La_2Zr_{2-y}Pu_yO_7$ ($0 \leq y \leq 2$). J Nucl Mater. 2015;466:162–71.
28. Li PC, Zhao FG, Xiao HY, et al. First-Principles Study of Thermo-Physical Properties of Pu-Containing $Gd_2Zr_2O_7$. Nanomaterials. 2019;9(2).
29. Zhang S, Li M, Xiao H, Liu Z-J, Zu X. A Comparative Study of Electron Radiation Responses of $Pu_2Zr_2O_7$ and $La_2Zr_2O_7$: An abinitio Molecular Dynamics Study. Materials. 2021;14(6): 1516.
30. Weber WJ, Ewing RC, Catlow CRA, De La Rubia TD, Hobbs LW, Kinoshita C, et al. Radiation effects in crystalline ceramics for the immobilization of high-level nuclear waste and plutonium. J Mater Res. 1998;13(6):1434–84.
31. Taylor CA, Patel MK, Aguiar JA, Zhang Y, Crespillo ML, Wen J, et al. Bubble formation and lattice parameter changes resulting from He irradiation of defect-fluorite $Gd_2Zr_2O_7$. Acta Mater. 2016;115:115–22.
32. Danielson T, Hin C. Structural and electronic effects of helium interstitials in $Y_2Ti_2O_7$: A first-principles study. J Nucl Mater. 2014;452(1):189–96.
33. Li X, Lu Y, Peng Q, Liu Y, Yang K, Xu C, et al. Ab initio investigation of properties and mobility of helium defects in $La_2Sn_2O_7$ pyrochlore. Nucl Mater Energy. 2022;30:101135.
34. Zhu C, Ding B, Yang D, Li Y, Liu C. Comparative study on the radiation resistance of pure and He-doped $Gd_2Zr_2O_7$ pyrochlore by DFT + U calculation. Nucl Instrum Methods Phys Res, Sect B. 2022;516:8–14.
35. Liu CG, Li YH, Li YD, Dong LY, Wen J, Yang DY, et al. First principle calculation of helium in $La_2Zr_2O_7$: Effects on structural, electronic properties and radiation tolerance. J Nucl Mater. 2018;500:72–80.
36. Kresse G, Hafner J. Ab initio molecular dynamics for liquid metals. Phys Rev B Condens Matter. 1993;47(1):558–61.
37. Kresse G, Hafner J. Ab initio molecular-dynamics simulation of the liquid-metal-amorphous-semiconductor transition in germanium. Phys Rev B Condens Matter. 1994;49(20):14251–69.
38. Kresse G, Furthmüller J. Efficiency of ab-initio total energy calculations for metals and semiconductors using a plane-wave basis set. Comput Mater Sci. 1996;6(1):15–50.
39. Kresse G, Furthmüller J. Efficient iterative schemes for ab initio total-energy calculations using a plane-wave basis set. Phys Rev B Condens Matter. 1996;54(16):11169–86.
40. Blöchl PE. Projector augmented-wave method. Phys Rev B Condens Matter. 1994;50(24):17953–79.
41. Kresse G, Joubert D. From ultrasoft pseudopotentials to the projector augmented-wave method. Phys Rev B. 1999;59(3):1758–75.
42. Perdew JP, Burke K, Ernzerhof M. Generalized gradient approximation made simple. Phys Rev Lett. 1996;77(18):3865–68.
43. Subramanian MA, Aravamudan G, Subba Rao GV. Oxide pyrochlores—a review. Prog Solid State Chem. 1983;15(2):55–143.
44. Lian J, Wang LM, Chen J, et al. Heavy Ion Irradiation of Zirconate Pyrochlores. MRS Proceedings. 2011:713;JJ11.35.
45. Lian J, Chen J, Wang LM, Ewing RC, Farmer JM, Boatner LA, et al. Radiation-induced amorphization of rare-earth titanate pyrochlores. Phys Rev B. 2003;68(13).
46. Wang XJ, Xiao HY, Zu XT, Weber WJ. A DFT+U study of cerium solubility in $La_2Zr_2O_7$. J Nucl Mater. 2012;424(1-3):69–74.
47. Chartier A, Meis C, Weber WJ, Corrales LR. Theoretical study of disorder in Ti-substituted $La_2Zr_2O_7$. Phys Rev B. 2002;65(13).
48. Yang L, Jiang Y, Robert Odette G, Yamamoto T, Liu Z, Liu Y. Trapping helium in $Y_2Ti_2O_7$ compared to in matrix iron: A first principles study. J Appl Phys. 2014;115(14).
49. Tsuchiya B, Yamamoto T, Ohsawa K, Odette GR. First-principles calculation of formation energies and electronic structures of hydrogen defects at tetrahedral and octahedral interstitial sites in pyrochlore-type $Y_2Ti_2O_7$ oxide. J Alloys Compd. 2016;678:153–59.
50. Crocombette J-P, Chartier A, Weber WJ. Atomistic simulation of amorphization thermokinetics in lanthanum pyrozirconate. Appl Phys Lett. 2006;88(5).
51. Lian J, Zu XT, Kutty KVG, Chen J, Wang LM, Ewing RC. Ion-irradiation-induced amorphization of $La_2Zr_2O_7$ pyrochlore. Phys Rev B. 2002;66(5).
52. Minervini L, Grimes RW, Sickafus KE. Disorder in Pyrochlore Oxides. J Am Ceram Soc. 2000;83(8):1873–78.
53. Henkelman G, Arnaldsson A, Jónsson H. A fast and robust algorithm for Bader decomposition of charge density. Comput Mater Sci. 2006;36(3):354–60.
54. Sanville E, Kenny SD, Smith R, Henkelman G. Improved grid-based algorithm for Bader charge allocation. J Comput Chem. 2007;28(5):899–908.
55. Tang W, Sanville E, Henkelman G. A grid-based Bader analysis algorithm without lattice bias. J Phys Condens Matter. 2009;21(8):084204.
56. Becke AD, Edgecombe KE. A simple measure of electron localization in atomic and molecular systems. J Chem Phys. 1990;92(9):5397–403.
57. Trachenko K. Understanding resistance to amorphization by radiation damage. J Phys Condens Matter. 2004;16(49):R1491–515.
58. Li Y, Kowalski PM, Beridze G, Birnie AR, Finkeldei S, Bosbach D. Defect formation energies in $A_2B_2O_7$ pyrochlores. Scr Mater. 2015;107:18–21.
59. Xia Y, Liu CG, Yang DY, Wen J, Liu H, Mu PC, et al. Synthesis and radiation tolerance of $Lu_{2-x}Ce_xTi_2O_7$ pyrochlores. J Nucl Mater. 2016;480:182–88.
60. Yang DY, Xu CP, Fu EG, Wen J, Liu CG, Zhang KQ, et al. Structure and radiation effect of Er-stuffed pyrochlore $Er_2(Ti_{2-x}Er_x)O_{7-x/2}$ (x = 0-0.667). Nucl Instrum Methods Phys Res, Sect B. 2015;356–357:69–74.
61. Li YH, Uberuaga BP, Jiang C, Choudhury S, Valdez JA, Patel MK, et al. Role of antisite disorder on preamorphization swelling in titanate pyrochlores. Phys Rev Lett. 2012;108(19): 195504.
62. Panero WR, Stixrude L, Ewing RC. First-principles calculation of defect-formation energies in the $Y_2(Ti,Sn,Zr)_2O_7$ pyrochlore. Phys Rev B. 2004;70(5).
63. Wei G, Zuo Y, Luo F, Yuan W, Dong F, Liu Yi, et al. Investigation of mechanical and thermodynamic properties of $La_2Zr_2O_7$ pyrochlore. Int J Energy Res. 2022;46(2):2011–20.

How to cite this article: Liu C, Gao R, Xia X, Yang K, Liu Y, Yang P, et al. First-principles study of helium incorporation in Pu-$La_2Zr_2O_7$ pyrochlore. J Am Ceram Soc. 2025;108:e20119. https://doi.org/10.1111/jace.20119